Journal of Electroanalytical Chemistry 717–718 (2014) 231–236

Contents lists available at ScienceDirect

Journal of Electroanalytical Chemistry

journal homepage: www.elsevier.com/locate/jelechem

Ethanol vs. glycerol: Understanding the lack of correlation between the oxidation currents and the production of CO_2 on Pt nanoparticles

Cauê A. Martins [a,*], Pablo S. Fernández [b], Horacio E. Troiani [c], María E. Martins [b], Giuseppe A. Camara [a,*]

[a] Institute of Chemistry/UFMS, C.P. 549, 79070-900 Campo Grande, MS, Brazil
[b] INIFTA, Facultad de Ciencias Exactas, UNLP, CCT La Plata – CONICET, (1900) La Plata, Argentina
[c] División Metales, Centro Atómico Bariloche, Av. Ezequiel Bustillo 9500, San Carlos de Bariloche, (8400) RN, Argentina

ARTICLE INFO

Article history:
Received 8 November 2013
Received in revised form 24 January 2014
Accepted 28 January 2014
Available online 4 February 2014

Keywords:
Ethanol
Glycerin
Oxidation pathways
Platinum nanomaterials
Direct alcohol fuel cells

ABSTRACT

In the last decades ethanol and glycerol arose as potential fuels for fuel cells. Based on their importance to the field and molecular similarity, here we compare the electrooxidation of ethanol and glycerol on platinum nanoparticles as an attempt to learn about their differences and similarities in terms of oxidation pathways. By using in situ FTIR we interpret the electrochemical behavior in terms of different pathways involving the production of carboxylic acids for both alcohols. For ethanol, CO_2 is produced from CO in a direct pathway involving several electrons, while acetic acid is produced through a parallel pathway. Conversely, for glycerol CO_2 seems to be mainly produced through a sequential pathway involving carboxylic acids, each one involving few electrons. The results suggest that glycerol demands surfaces that speed up the oxidation of partially oxidized species formed at intermediate potentials.

1. Introduction

In the last decades, the development of direct alcohol fuel cells (DAFCs) – particularly those fed with methanol, ethanol and glycerol – has attracted an increasing number of researchers [1–3]. Ethanol and glycerol present an especial environmental interest. Ethanol can be produced in large scale from biomass, and it is less toxic than methanol [4]. On the other hand, glycerol is also a potential candidate to be used as fuel in fuel cells, due to its high theoretical energy and availability as a co-product of biodiesel fabrication. In part, the collective effort to study these compounds has been motivated by the difficulty to use alcohols of small chain in fuel cells in an efficient way. The hindrance to extract the energy available in an alcohol is mostly caused by parallel reactions, mainly due to the poor ability of metallic surfaces to promote the cleavage of C—C bonds. Consequently, we observe the formation of partially oxidized products of intact chain, with a clear commitment of the energetic efficiency of the whole system [3].

Apparently, the efficiency in breaking C—C bonds can be inferred by the presence of CO_2, once its production means that the alcohol was fully oxidized, thus providing the maximum available energy. In this context, there are several works devoted to the electrooxidation of ethanol [5,6] and glycerol [7–9]. However, at least to our knowledge, there are no studies devoted to compare the energetic throughput between these alcohols, based on the CO_2 production and electrochemical current density. This issue is the main concern of this work.

Herein we present a comparative study of ethanol and glycerol electrooxidation on Pt nanoparticles (NPs) in acidic media. In order to relate the magnitude of C—C cleavage with the electroactivity of Pt NPs we followed both oxidation reactions by in situ FTIR. Results show that the electrochemical behavior cannot be fully understood by the production of CO_2, and different pathways of oxidation, each one involving a few electrons, must be considered to understand the current × time curves behavior for both alcohols.

2. Materials and methods

2.1. Electrodes, chemicals and synthesis of platinum nanoparticles

Pt NPs dispersed on carbon Vulcan® XC-72R were synthesized as described elsewhere [10]. Shortly, appropriate amounts of $H_2PtCl_6{\cdot}6H_2O$, Vulcan® XC-72R and polyvinylpyrrolidone (PVP) were mixed to an ethylene glycol/water 3:1 (V/V) solution and heated for 2 h. The PVP/metal molar ratio was set to 0.3 and the resultant powder contained 40% of Pt/C (w/w). The dispersion was washed with water followed by centrifugation under 4500 rpm for 1 h. The supernatant was discarded and the process was repeated five times. The remaining dispersion was dried at 60 °C during 24 h on oven. Afterwards, an ink was prepared by adding 1 mg of Pt/C

* Corresponding authors. Tel.: +55 67 3345 3576; fax: +55 67 3345 3552.
E-mail addresses: cauealvesmartins@gmail.com (C.A. Martins), giuseppe.silva@ufms.br (G.A. Camara).

http://dx.doi.org/10.1016/j.jelechem.2014.01.027
1572-6657/

into 2 mL of 2-propanol and 50 μL Nafion® 5%. Finally, the mixture was sonicated for 30 min to homogenize the dispersion.

A polycrystalline gold disk with 0.79 cm^2 of geometric area was used as substrate to adhere the NPs. The disk was polished to a mirror finish and heated in a plate at 50 ± 2 °C. Then, aliquots of 50 μL of ink and 50 μL of diluted Nafion® solution (1 mL of Nafion® 5%:20 mL of 2-propanol) were applied over the disk. Before each experiment, the electrode was washed with water to pull out those particles not well adhered.

Solutions were prepared with Milli-Q® water (18.2 MΩ cm), glycerol 99.5% (Labsynth p.a), ethanol (Merck) and $HClO_4$ (Suprapur, Merck). Nitrogen of high purity was used to purge the solutions before and during the experiments. The counter electrode was a Pt sheet of high geometric area. All potentials were measured against a reversible hydrogen electrode (RHE) in 0.1 mol dm^{-3} $HClO_4$.

2.2. Techniques

After being transferred to the electrochemical cell, the state of the electrode surface was checked by potential cycling between 0.05 and 1.50 V. We have also used cyclic voltammetry to check the electrochemical response in presence of the alcohols between 0.05 and 1.45 V at 0.02 V s^{-1}. Currents were normalized by the electrochemically active surface area calculated in function of the charge involved in the hydrogen desorption [11]. Afterwards, ethanol or glycerol was admitted into the cell in concentrations of 75 and 50 mmol dm^{-3}, respectively. A concentration ratio of 3/2 (ethanol/glycerol) was used to provide the same number of carbon atoms in both situations, since ethanol and glycerol have two and three carbons in their respective chains. Next, $i \times t$ curves were obtained for both alcohols by applying successive potential steps of 0.05 V from 0.05 to 1.45 V, holding each potential for 300 s.

In situ FTIR experiments were performed in a spectrometer coupled to a MCT detector in presence of the alcohols in 0.1 mol dm^{-3} $HClO_4$ solutions. The spectroelectrochemical cell was fitted with a CaF_2 planar window (3000–1000 cm^{-1}) and is described elsewhere [12]. Reflectance spectra were collected as the ratio (R/R_0) where R represents a sample spectrum while R_0 was collected at 0.05 V. Spectra were computed from 50 interferograms averaged, being collected at intervals of 0.05 V between 0.05 and 1.45 V. The spectral resolution was set to 8 cm^{-1}. Positive and negative bands represent the consumption and production of substances, respectively. The system was kept at 0.05 V during 45 min before each experiment, in order to obtain a stable thin layer. For that, all the experiments were initialized with approximately the same IR signal intensities, which indicates that the absorption by the solvent inside the thin layer is similar in successive experiments, as suggested in a previous work [13].

Transmission electron microscopy (TEM) and high-resolution transmission electron microscopy (HRTEM) experiments were performed in a CM 200 Philips microscope operated at 200 keV and equipped with a LaB_6 emission gun and an ultratwin objective lens. X-ray diffraction patterns (XRD) were obtained with a Miniflex II model Rigaku diffractometer using Cu Kα radiation (λ = 0.15406 nm). Diffraction data were collected by step scanning with a step size of 0.02° 2θ in the range 5–90°, with a scan step of 2 s.

3. Results and discussion

3.1. Characterization of platinum nanoparticles

Fig. 1 shows the TEM (Fig. 1A) and HR-TEM (Fig. 1B) images, respectively, for Pt NPs and the corresponding histogram (Fig. 1C). It can be observed that the metal nanoparticles (dark spots) have heterogeneous geometry. Most particles are spherical, but some are irregular. Overall, the particles are fairly dispersed on the carbon support (brighter region). The histogram shows NPs with a narrow size distribution, with most of particles in the range of 2.0–4.0 nm. The average particle diameter (estimated from ~200 particles) was 2.74 ± 0.04 nm.

The XRD pattern for Pt NPs, Fig. 1D, shows the characteristic peaks of the face-centered cubic structure (fcc). The C(002) reflection confirms the presence of graphitic planes in the structure of carbon Vulcan® XC-72. Other diffraction peaks correspond to Pt (111), (200), (220) and (311) planes and are observed at 2θ values of 40°, 47°, 67° and 82°, respectively. From Bragg equation we estimated the Pt lattice parameter as 0.395 nm, in reasonable agreement with that reported by You et al. [14]. Peaks in Fig. 1D show a broad feature, which is probably due to the small particles size. Based on the peak broadening and using the Scherrer equation we estimated the size of the crystallites. The size calculated for each corresponding reflection was 2.43 nm (111), 2.76 nm (200), 2.63 nm (220) and 2.32 nm (311). These results are fairly consistent with the values obtained from the TEM images of the same samples and indicate that most particles are probably single crystals. At this point, is important to note that these results can be interpreted as a representative behavior of regular, non-orientated Pt NPs. This feature is important once we are dealing with a system that is similar to those usually found in fuel cells.

3.2. Electrooxidation of ethanol and glycerol on platinum

Fig. 2A shows the cyclic voltammograms in presence of ethanol (black line) and glycerol (red line) on Pt NPs. For ethanol, two oxidation peaks, centered at ca. 0.9 and 1.3 V (E_I and E_{II}), are observed during the positive-going scan and a reactivation peak at 0.7 V (E_{III}), is observed on the negative-going scan [5,6]. The voltammogram obtained in presence of glycerol presents a broad peak composed of two overlapping peaks, with maximum currents at 0.75 and at ~0.8 V [13,15]. Afterward, the current diminishes and increases again, reaching a new maximum at the vertex potential (G_{II}). During the negative-going scan, the anodic currents experience an abrupt decrease, reaching negligible values at 1.1 V, where no oxidation current is observed. Finally, a sudden reactivation of the surface is observed at around 0.8 V (G_{III}) [13,15].

The first peaks of ethanol electrooxidation reaction (EEOR) and glycerol electrooxidation reaction (GEOR) have approximately the same onset potential. However, current density of E_I is higher than G_I (Fig. 2A). The second anodic peaks also present similar onset potential and G_{II} keeps increasing up to the vertex potential, while E_{II} shows a well-defined peak. E_{II} displays superior current until it is intercepted by G_{II} at 1.37 V. This narrow potential range is the only one in which GEOR generates higher current densities than EEOR.

The electrochemical behavior of ethanol on Pt/C and smooth Pt is similar, as shown by Fig. S1. Otherwise, GEOR presents a remarkable difference on peak I for both catalysts (Fig. S1). Peak I shows a large shoulder (two overlapping peaks at ~0.75 and at ~0.8 V) on Pt/C during the positive scan. Meanwhile, this potential region on smooth Pt displays two well-defined peaks, at ~0.73 and 0.77 V (Fig. S1 A). This difference can be explained as a specific contribution of the Pt (111) sites. Gomes et al. reported the GEOR on Pt (111) in $HClO_4$ medium and they found two well defined peaks at similar potentials [9]. It is well known that when a Pt polycrystalline electrode is annealed, most the surface reconstructs towards the atomic arrangement with lowest surface energy, i.e., Pt (111) sites. Therefore, when hydrogen (or butane) flame is used to clean a Pt electrode before the experiments, the two maxima of current in GEOR peak I appear better defined, as shown here (Fig. S1 A) and in the literature [7,13,15]. On the other hand, Pt NPs without preferential orientation show a shoulder (Fig. 1A),

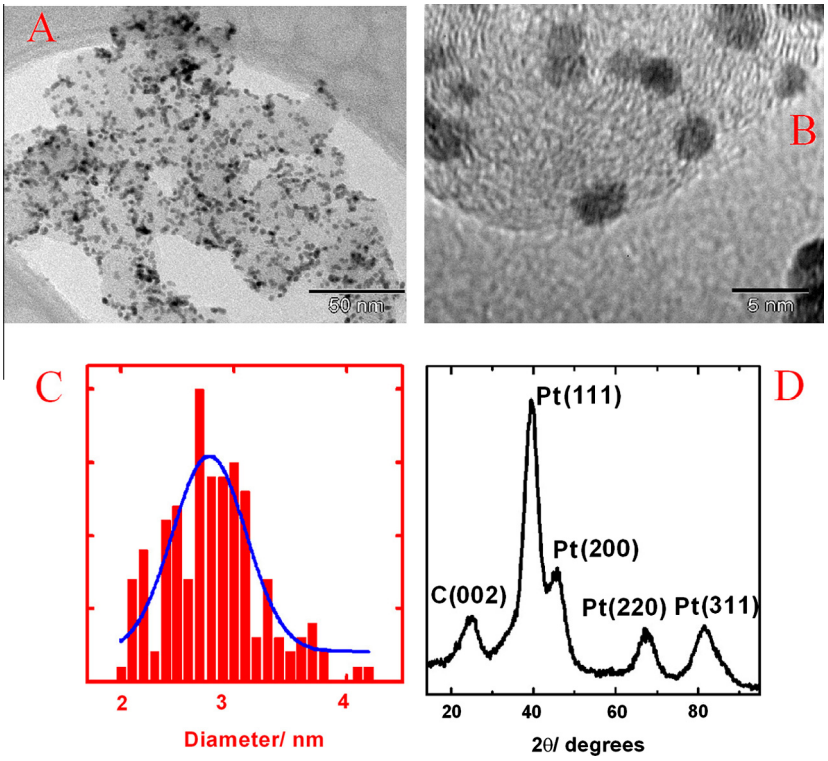

Fig. 1. Physical characterization of carbon supported platinum nanoparticles, consisting of A: TEM images; B: HR-TEM images; C: histograms; D: XRD spectra.

which is also in agreement with the literature [16,17]. The previous treatment of bulk Pt electrodes might be the reason for the distinct voltammetric profiles of GEOR found in the literature. In this sense, Pt/C NPs seems to be the right option for the spectroelectrochemical study because there is no relevant contribution of a specific site, and the results can be interpreted as a representative behavior of non-orientated Pt NPs.

Based in previous works, we can argue that the electrooxidation of glycerol generates important moieties of CO_2 [15] and other intermediates [8,9,13,16] while ethanol produces mainly acetic acid and glyceraldehyde during its electrooxidation in acidic medium [5,6]. Based on these findings, it is reasonable to expect that the greater production of CO_2 would generate higher currents for glycerol, but this is not we observed in Fig. 2A. Namely, the currents generated from ethanol electrooxidation are dominant at long of the whole cycle (except for potentials up to 1.37 V, as discussed). This result suggests that the interpretation of the cyclic voltammogram is a little more subtle than we intend. These findings will be further discussed in terms of chronoamperometric experiments in the next section.

Next, we followed both the oxidation reactions by in situ FTIR in an attempt to understand the corresponding electrochemical responses in terms of their oxidation pathways. Figs. 2B and C show illustrative spectra obtained during the electro-oxidation of ethanol and glycerol, respectively. Further details about the assignment of bands of ethanol can be consulted in [5,6,18]. Details about bands in presence of glycerol are described in [6–8,13,16]. Briefly, Figs. 2B and C show a well-defined CO_2 band (2343 cm^{-1}) starting at ~0.6 V and a band at about 2030 cm^{-1} corresponding to adsorbed CO. Fig. 2B shows bands at 1715, 1401, 1360, 1283 and 1100 cm^{-1}, related to —CO stretching of carbonyl compounds, CH_3 symmetric bending of acetaldehyde, —COOH group of acetic acid and perchlorate, respectively. On the other hand, spectra obtained during the electrooxidation of glycerol (Fig. 2C) show bands at 2343 and 1733 cm^{-1} corresponding to C=O stretching of CO_2 and carbonyl groups, respectively. Also, a wide band composed by two vibration modes (1122 + 1100 cm^{-1}) is due to the superimposition of a C—O stretching of glyceraldehyde and a Cl—O stretching of perchlorate. Here is important to highlight that a spectrum of glycerol electrooxidation contains more bands than the ones discussed here, but due to their low intensity these bands are hard to discriminate.

3.3. The correlation between the oxidation currents and the production of CO_2 on Pt nanoparticles

The integrated bands of CO_2 produced from ethanol and glycerol are shown in Fig. 3. The CO_2 bands are detectable at 0.55 V and increase up to 0.9 V. The CO_2 signal from ethanol slightly decreases from 0.9 up to 1.45 V, while the CO_2 from glycerol abruptly increases.

Aiming to deepen the present discussion and understand the differences in the current profiles, we followed the quasi-stationary currents (QSC) obtained in presence of ethanol and glycerol by in situ FTIR, as shows Fig. 4. The use of potential steps minimizes the influence of transient effects caused by potential changes and provides a better correlation between FTIR spectra and electrochemical currents. The profiles of QSCs (Fig. 4) are different to those of the voltammograms (Fig. 2A), probably because the conditions adopted in QSC method (potential steps) allow the accumulation of intermediates/products of slow kinetics in the surroundings of the electrode. Once potential steps were also used during the acquisition of spectra, this comparison seems to be more meaningful than that made with the voltammograms. Representative spectra for both alcohols are shown for selected potentials in Fig. 4. Before the analysis, is important noting that the experimental conditions were strictly controlled, including the gold surface polish and the mass of catalyst deposited on it, allowing the comparison of the subsequent experimental data.

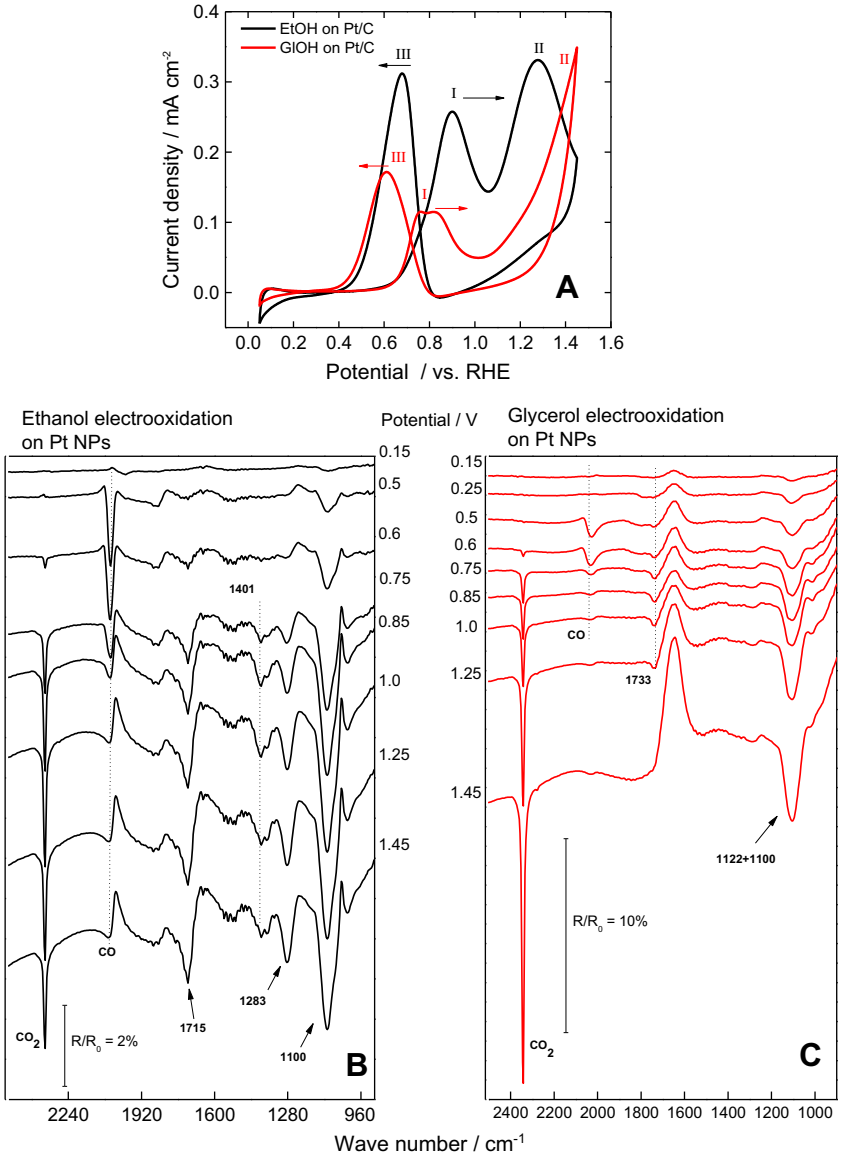

Fig. 2. (A) Cyclic voltammograms in presence of ethanol 75 mmol dm^{-3} (black line) and glycerol 50 mmol dm^{-3} (red line) in $HClO_4$ 0.1 mol dm^{-3} at 0.02 Vs^{-1}. 2(B) and (C) shows in situ FTIR spectra obtained during the electrooxidation of ethanol and glycerol, respectively, on Pt/C nanoparticles. The potential of each spectrum is shown in figure. (For interpretation of the references to colour in this figure legend, the reader is referred to the web version of this article.)

Fig 4 shows that QSCs for both alcohols start to increase at ~0.45 V, but in general, the currents for glycerol are lower than for ethanol, especially above 0.6 V. At this potential the CO_2 band (2343 cm^{-1}) becomes detectable for both alcohols. The corresponding bands are of similar magnitude, indicating that the production of CO_2 is nearly the same in both situations, although the formation of CO (bands ~2030 cm^{-1}) seems to be more intense for ethanol than for glycerol. For glycerol, the currents reach a plateau between 0.6 and 0.85 V, while for ethanol they grow sensibly in that potential range, reaching a peak at 0.85 V.

Coming back to FTIR spectra, at 0.85 V the amounts of CO_2 remain similar for both alcohols, but the oxidation wave for ethanol at this potential is four times higher than for glycerol. Hence, the currents observed for ethanol cannot be explained olely by the production of CO_2. Ergo, some other species must be (at least partially) responsible for the rising currents of ethanol in Fig. 4. The comparison of the spectra at 0.85 V shows that for ethanol a well-developed band is seen at 1283 cm^{-1}, due the formation of acetic acid, which is a dominant pathway of ethanol electrooxidation [5,6]. On the other hand, only an ill-defined band is noted for glycerol, suggesting that the formation of the corresponding carboxylic acid is incipient for this alcohol.

Furthermore, after the maximum (0.85 V) the currents of ethanol electrooxidation abruptly decrease. In contrast, the glycerol QSC experiences a second increase, beginning at 1.0 V and persisting up to 1.45 V. Meanwhile, the production of CO_2 becomes the major feature of the spectrum of glycerol. At the end of the QSC curve, the currents for glycerol are still growing. Correspondingly, at this potential the CO_2 signal is six times more intense for glycerol than for ethanol. At this point, a question remains to be clarified: If the CO_2 pathway is the one which involves the major number of electrons how to explain the lack of correlation between its production and the QSC signals for both alcohols?

First of all, the spectrum at 0.85 V shows that the formation of CO_2 does not explain the oxidation currents for ethanol. As argued, acetic acid also contributes to those currents. A second point is that during the electrooxidation of ethanol CO_2 is produced mainly from adsorbed CO (acetic acid is an end product of ethanol

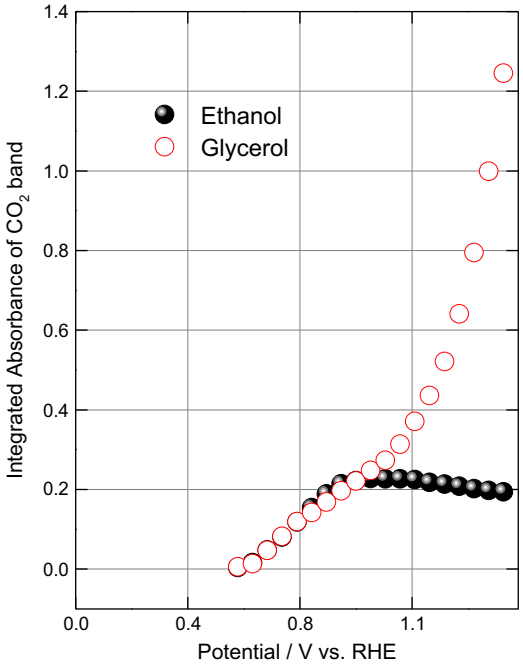

Fig. 3. Integrated absorbance of CO_2 band from ethanol and glycerol extracted from spectra like those shown in Fig. 2.

oxidation [5]). Hence, each cycle of production of CO_2 from ethanol implies that 12 electrons are released to the surface, assuming that both groups (CH_3 and CH_2OH) are able to generate CO_2 [19]. Ergo, for ethanol there are two parallel branches of oxidation, both contributing to the emergence of currents observed in Fig. 4 (and also in Fig. 2A).

Conversely, for glycerol the relative low CO signals and the high potentials required for the production of CO_2 suggest that the main pathway for its formation involves the oxidation of carboxylic acids. Indeed, in a recent publication we suggested that glyceraldehyde is an intermediate of CO_2 and glyceric acid [20]. If this is the case, most of CO_2 is expected to be formed through an indirect mechanism, with each oxidation step involving only a few electrons. This assumption explains why the massive production of CO_2 (from glycerol) does not imply in high currents. It is simply because CO_2 is mainly formed from partially oxidized intermediates. In this context, as glycerol is a molecule more oxygenated than ethanol, its oxidation to intermediates as glycolic and formic acid is easier than the cleavage of the C—C bond in ethanol. Furthermore, it seems reasonable to assume that at least part of these species remain adsorbed on the surface until they are oxidized to CO_2 which could explain the relative low coverage by CO observed for glycerol. At potentials higher than 1.1 V, important amounts of intermediates from GEOR seem to be oxidized to CO_2 generating high currents (but still far from the maximum observed for EEOR), while the final products from ethanol leave the thin layer (as shown by current decay of Fig. 1A).

In conclusion, although glycerol produces more CO_2 per mass, this does not imply in higher oxidation currents, apparently because the oxidation pathways that culminate with the formation of CO_2 appear to be slower (mainly because they involve several steps, each one delivering only a few electrons) than the corresponding ones for ethanol. Based on these assumptions, it becomes clear that the electrooxidation of glycerol is too complex for a single metallic catalyst. Hence, the search for catalysts able to electrooxidize glycerol efficiently should focus on new multifunctional surfaces that selectively drive the reaction towards

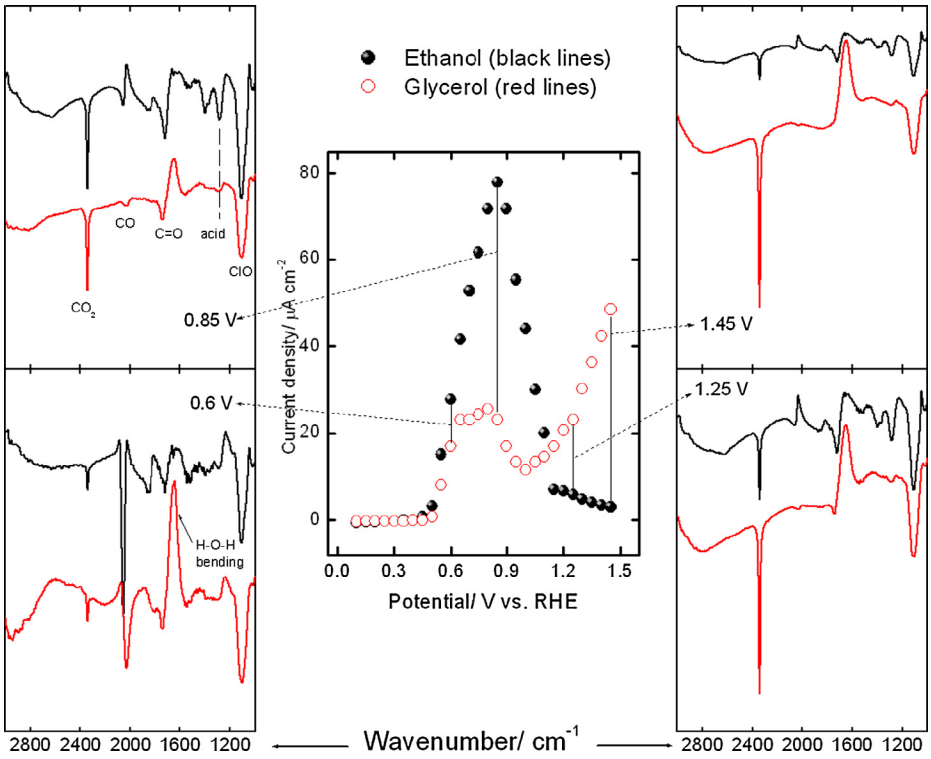

Fig. 4. Center: quasi-stationary currents for ethanol (full circles) and glycerol (open circles) on Pt NPs, obtained in 0.1 mol dm^{-3} $HClO_4$. Corners: FTIR spectra obtained for ethanol (black lines, upper curves) and glycerol (red lines, lower curves) in 0.1 mol dm^{-3} $HClO_4$. The potentials where the spectra were collected are indicated and correspond to the vertical bars in the central figure. (For interpretation of the references to colour in this figure legend, the reader is referred to the web version of this article.)

a CO_2 direct pathway and/or speed up the oxidation of those species formed at intermediate potentials.

4. Conclusions

- At intermediate potentials, glycerol and ethanol generate similar amounts of CO_2. However, the production of CO_2 does not explain the electrochemical results, since the oxidation currents for ethanol are higher than those for glycerol.
- These results are explained in terms of different pathways involving the production of carboxylic acids for both alcohols.
- For ethanol, CO_2 is produced from adsorbed CO in a direct pathway that involves several electrons; in a parallel pathway, acetic acid is the other final product of oxidation.
- Conversely, for glycerol most of CO_2 seems to be produced from partially oxidized intermediates and requires high potentials to occur. Moreover, the oxidation seems to follow a sequential, indirect pathway, with each oxidation step involving a few electrons.

Acknowledgements

The authors acknowledge financial assistance from CONICET, UNLP, CNPq, FUNDECT, CAPES and FINEP. Authors also thank Alejandra Floridia for taking HR-TEM images.

Appendix A. Supplementary data

Supplementary data associated with this article can be found, in the online version, at http://dx.doi.org/10.1016/j.jelechem.2014.01.027.

References

[1] C. Lamy, A. Lima, V. LeRhun, F. Delime, C. Countanceau, J.-M. Léger, J. Power Sources 105 (2002) 283–296.
[2] V. Bambagioni, C. Bianchini, A. Marchionni, J. Filippi, F. Vizza, J. Teddy, P. Serp, M. Zhiani, J. Power Sources 190 (2009) 241–251.
[3] T.J. Leo, M.A. Raso, E. Navarro, E. Sánchez-de-la-Blanca, J. Power Sources 196 (2011) 1178–1183.
[4] A. Demirbas, Progr. Energy Combust. Sci. 33 (2007) 1–18.
[5] M.J. Giz, G.A. Camara, J. Electroanal. Chem. 625 (2009) 117–122.
[6] G.A. Camara, T. Iwasita, J. Electroanal. Chem. 578 (2005) 315–321.
[7] P.S. Fernández, M.E. Martins, C.A. Martins, G.A. Camara, Electrochem. Commun. 15 (2012) 14–17.
[8] J. Schnaidt, M. Heinen, D. Denot, Z. Jusys, J. Behm, J. Electroanal. Chem. 661 (2011) 250–264.
[9] J.F. Gomes, F.B.C. de Paula, L.H.S. Gasparotto, G. Tremiliosi-Filho, Electrochim. Acta 76 (2012) 88–93.
[10] M. Chen, Y. Xing, Langmuir 21 (2005) 9334–9338.
[11] H.A. Kozlowska, in: E.B. Yeager, J.O'M. Bockris, B.E. Conway (Eds.), Comprehensive Treatise of Electrochemistry, vol. 9, Plenum Press, New York, 1984, p. 2.
[12] T. Iwasita, F.C. Nart, Progr. Surf. Sci. 55 (1997) 271–340.
[13] J.F. Gomes, C.A. Martins, M.J. Giz, G. Tremiliosi-Filho, G.A. Camara, J. Catal. 301 (2013) 154–161.
[14] V. Komanicky, A. Menzel, K.-C. Chang, H. You, J. Phys. Chem. B 109 (2005) 23543–23549.
[15] C.A. Martins, M.J. Giz, G.A. Camara, Electrochim. Acta 56 (2011) 4549–4553.
[16] P.S. Fernández, M.E. Martins, G.A. Camara, Electrochim. Acta 66 (2012) 180–187.
[17] P.S. Fernández, D.S. Ferreira, C.A. Martins, H.E. Troiani, G.A. Camara, M.E. Martins, Electrochim. Acta 98 (2013) 25–31.
[18] M.H. Shao, R.R. Adzic, Electrochim. Acta 50 (2005) 2415–2422.
[19] M.J.S. Farias, G.A. Camara, A.A. Tanaka, J. Solid State Electrochem. 11 (2007) 1465–1469.
[20] P.S. Fernández, C.A. Martins, M.E. Martins, G.A. Camara, Electrochim. Acta 112 (2013) 686–691.